Electronic Supporting Information

Strong Metal-Support Interaction in Copper Hexacyanoferrate Nanocubes Decorated Functionalized Multiwall Carbon Nanotubes for Enhanced Bi-functional Oxygen Electrocatalytic Activity and Stability

Priya Jain, Shwetambara Jha and Pravin P. Ingole*

Department of Chemistry, Indian Institute of Technology Delhi, New Delhi– 110016, India

Table S1: Comparison of ORR performance of Prussian blue based materials.

S.No.	Catalyst	Synthesis procedure	Electrolyte	E_{onset} (V)	$E_{1/2}$ (V)	J_{1600} rpm (mA cm^{-2})	N	Ref.
1.	CoFe-NC/NC	Pyrolysis of CoFePBA	0.1 M KOH	0.96V	0.85 V vs RHE	-	3.94-3.99	[1]
2.	Ni-HCF thin film	Chemical anodising	0.1 M KOH	0.685 V vs RHE	-	2.25	2-2.25	[2]
3.	PBC/C	Solid state pyrolysis of Fe-EDTA	0.1 M KOH	0.89 V vs RHE	-	6.4	3.8	[3]
4.	Cu/Fe/N-C	Pyrolysis of CuHCF and melamine precursors	50 mM PBS solution	0.12V (vs Ag/AgCl)	0.0 V vs Ag/AgCl	6.04	-	[4]
5.	PB/GE	Spontaneous redox synthesis	0.1 M H_2SO_4 + 0.1 M K_2SO_4	-0.2V vs SCE	-	-	4	[5]
6.	CdHCF	Anion exchange route	0.1 M KOH	0.84V vs RHE	-	-	2.37	[6]
7.	rGO-Pb/Pt	Sol gel aggregation	0.5 M H_2SO_4	-	-	-	3.9-3.95	[7]
8.	**CHF/*f*-CNT**	**Hydrothermal synthesis**	**0.1 M KOH**	**0.79V vs RHE**	**0.63V vs RHE**	**4**	**3.6-3.8**	**This study**

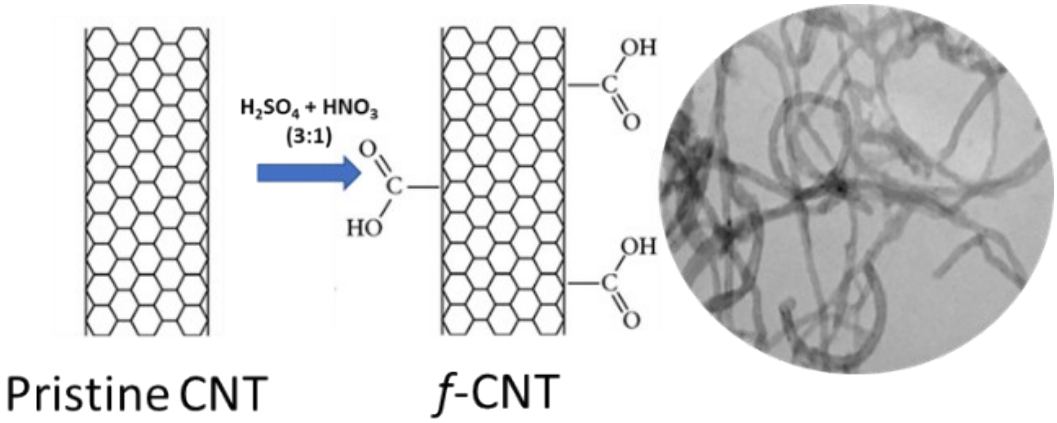

Scheme S1: A schematic representation of the functionalization of multi-walled carbon nanotubes.

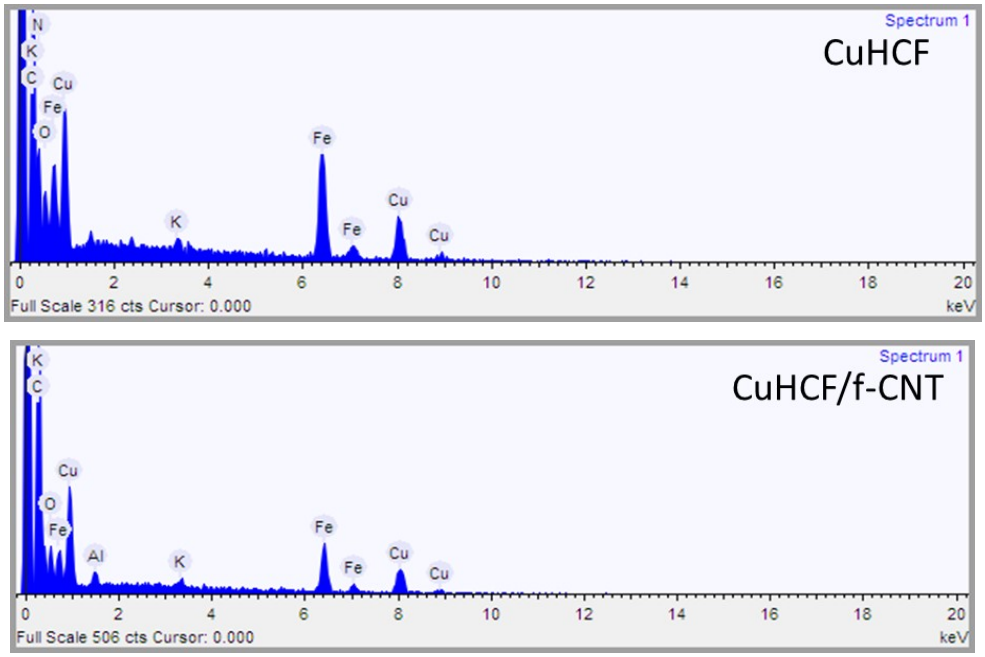

Fig. S1: The EDX spectra of CuHCF and CuHCF/f-CNT

Table S2: Chemical composition of MWCNTs samples in atomic %.

Element	**CuHCF**	**CuHCF/f-CNT**
Carbon	51.194	44.323
Nitrogen	29.845	34.724
Oxygen	13.335	13.507
Potassium	0.179	0.057
Iron	2.295	3.573
Copper	3.152	3.835

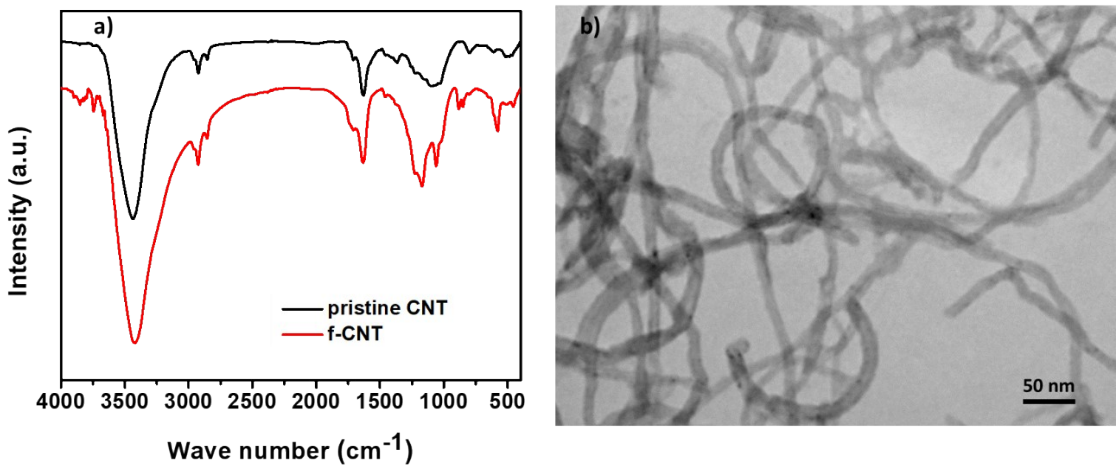

Fig. S2 a) FTIR of pristine MWCNT and *f*-MWCNT and **b)** TEM image of *f*-MWCNT.

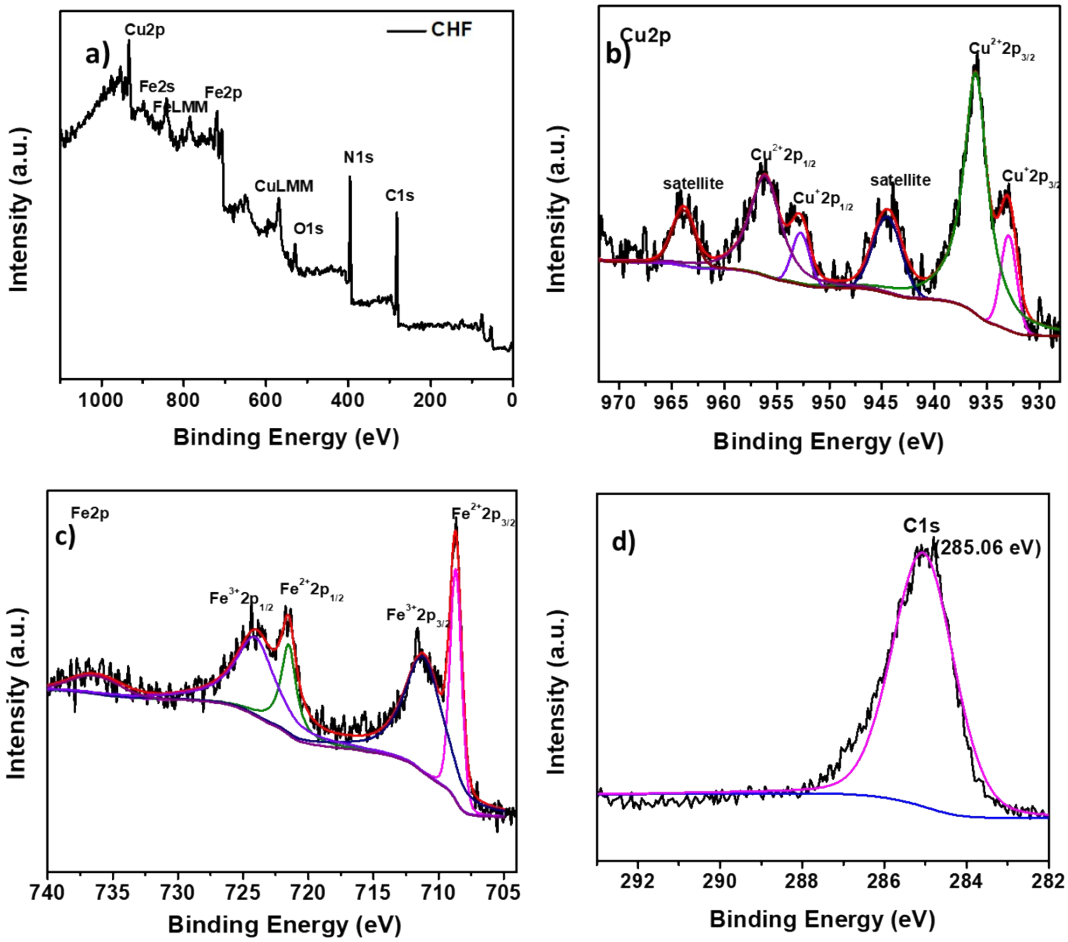

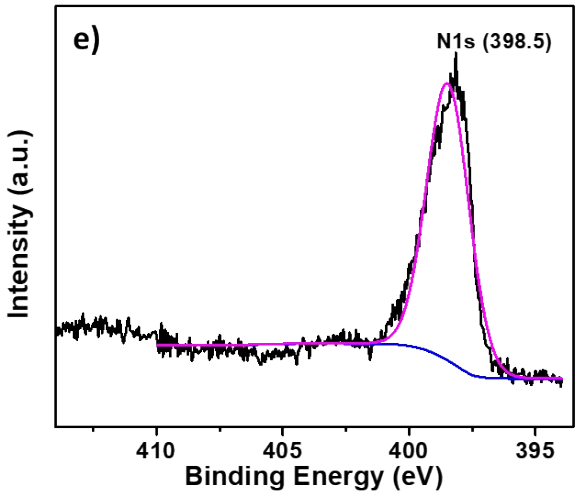

Fig. S3: XPS analysis of CuHCF, a) The survey spectrum and high resolution spectra of b) Cu2p, c) Fe2p, d) C1s and e) N1s.

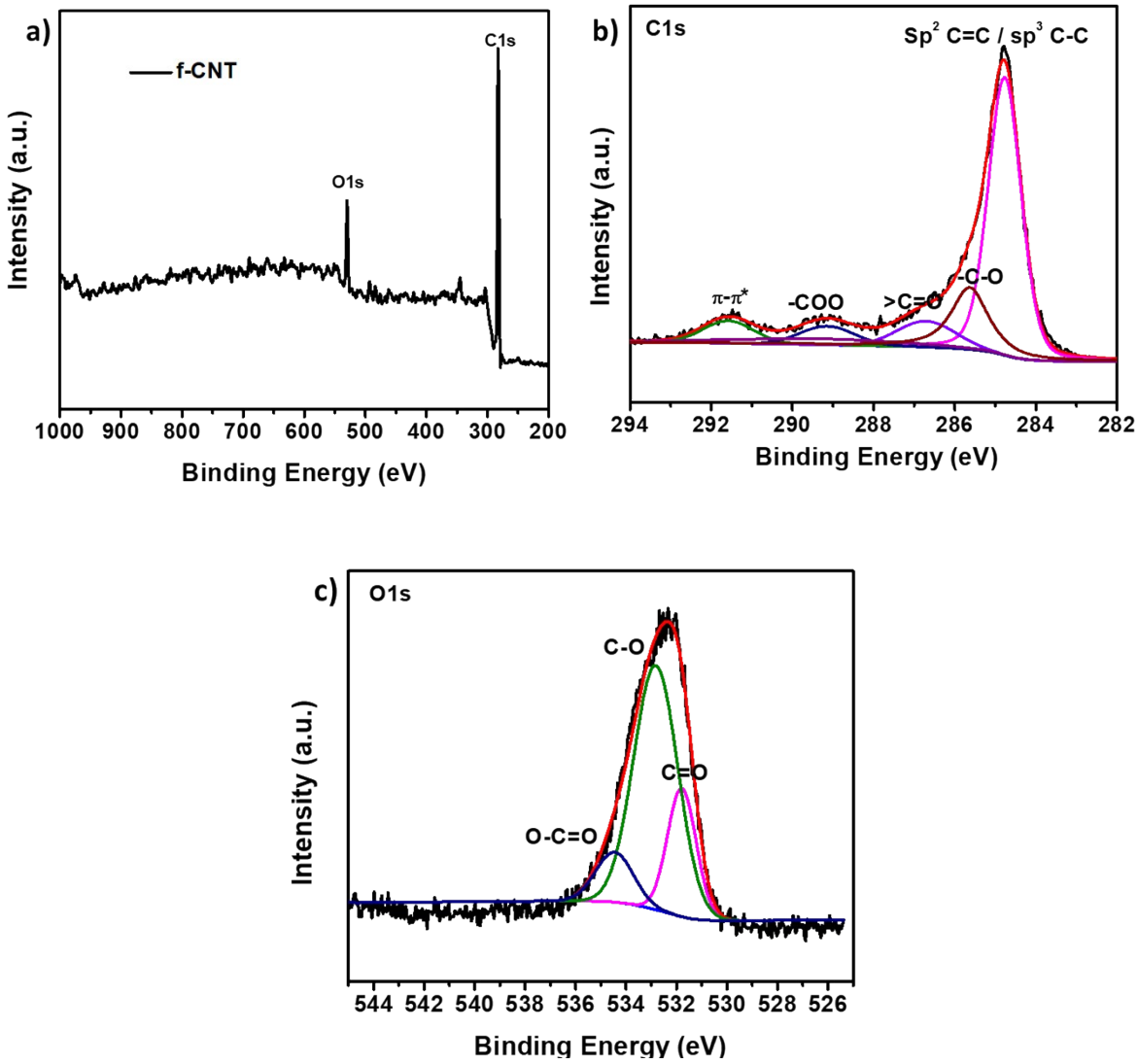

Fig. S4: XPS analysis of *f*-MWCNT, a) survey spectrum, the high resolution spectra of b) C1s and c) O1s.

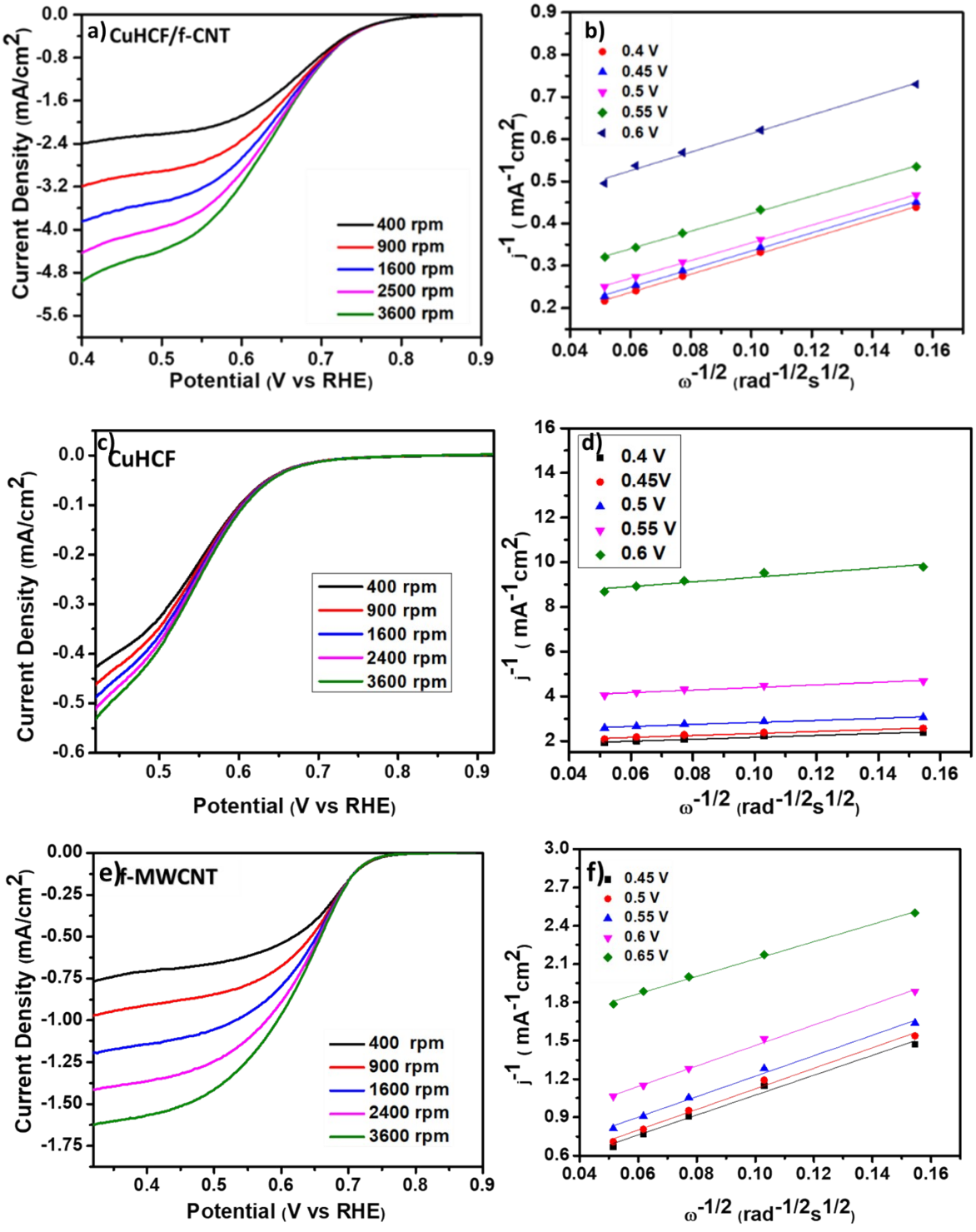

Fig. S5: RDE polarisation curve and corresponding K-L plots of a) and b) CuHCF/*f*-CNT, c) and d) CuHCF, and e) and f) *f*-MWCNT.

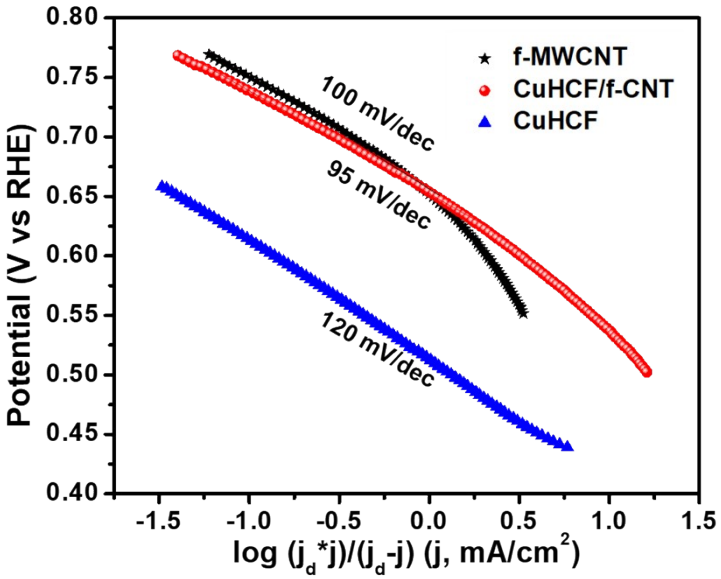

Fig. S6: Comparison of mass-transfer corrected Tafel slope of CuHCF, *f*-MWCNT and CuHCF/*f*-CNT.

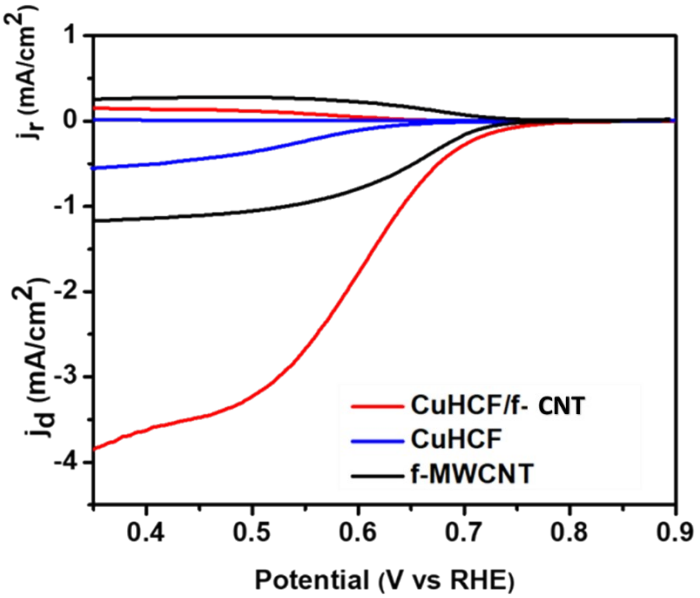

Fig. S7: RRDE comparison plot at 1600 rpm for CuHCF, *f*-MWCNT, and CuHCF/*f*-CNT.

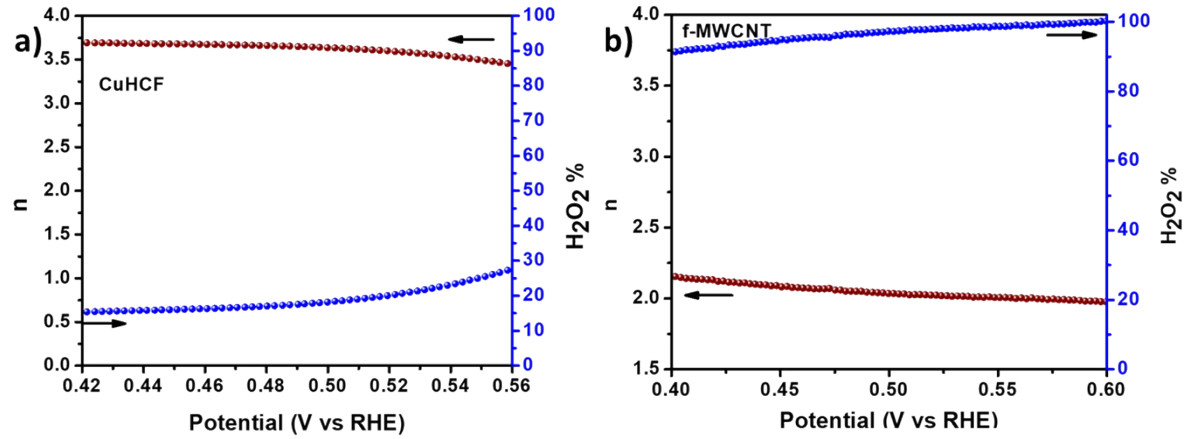

Fig. S8: The value of n and % H_2O_2 for a) CuHCF and b) *f*-MWCNT.

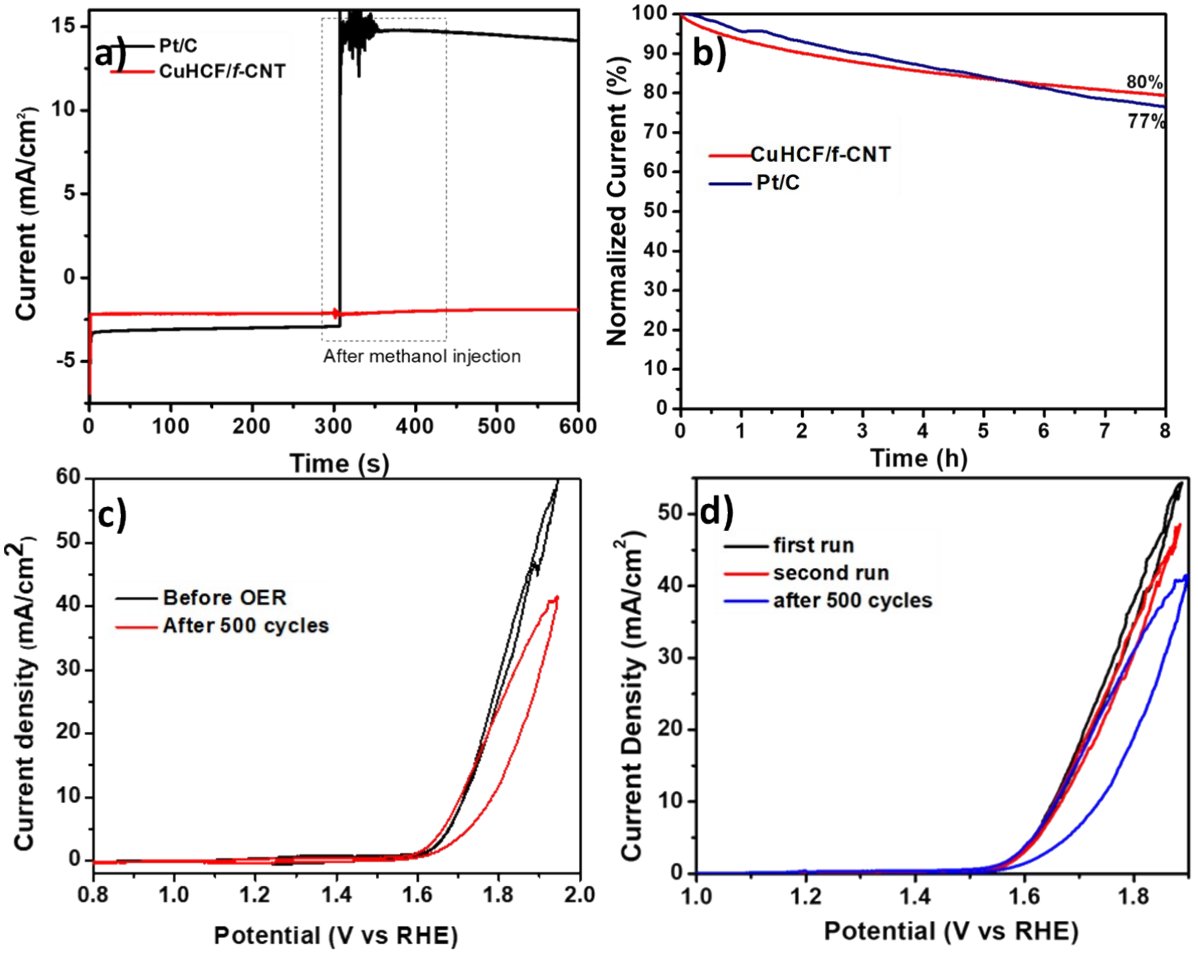

Fig. S9: a) The Chronoamperograms at 0.6 V vs RHE for CuHCF/f-CNT (red curve) and Pt/C (black curve) with addition of methanol at 300 s, **b)** The chronoamperograms at 0.6 V vs RHE for stability comparison for 8 hours for CuHCF/f-CNT and Pt/C (80 wt%), **c)** and **d)** The Cyclic voltammetry plot of CuHCF/*f*-CNT in 0.1M KOH solution before and after 500 CV cycles for OER stability.

Table S3: The comparison of ORR/OER electrocatalytic activity parameters for CuHCF, *f*-MWCNT and CuHCF/*f*-CNT.

	Material	CuHCF	*f*-MWCNT	CuHCF/*f*-CNT
ORR	**E_{onset} (V vs RHE)**	0.68	0.78	0.79
	$E_{1/2}$ (V vs RHE)	0.52	0.65	0.62
	n (0.5 V)	3.63	1.93	3.78
	% H_2O_2 (0.5 V)	18	99	15
	J_k (0.6V)(mA/cm^2)	0.12	0.68	2.56
	J_d (mAcm^{-2}) (0.4V)	0.5	1.16	3.4
	Tafel slope(mV/dec)	120	100	95
	α	0.49	0.59	0.62
	J_0 (mA/cm^2)	4.67×10^{-4}	1.83×10^{-3}	7.94×10^{-3}
	K^0 (cm/s)	4.84×10^{-5}	1.89×10^{-4}	8.22×10^{-4}
OER	**E_{onset} (V vs RHE)**	1.75	1.65	1.60
	Tafel slope(mV/dec)	165	105	86

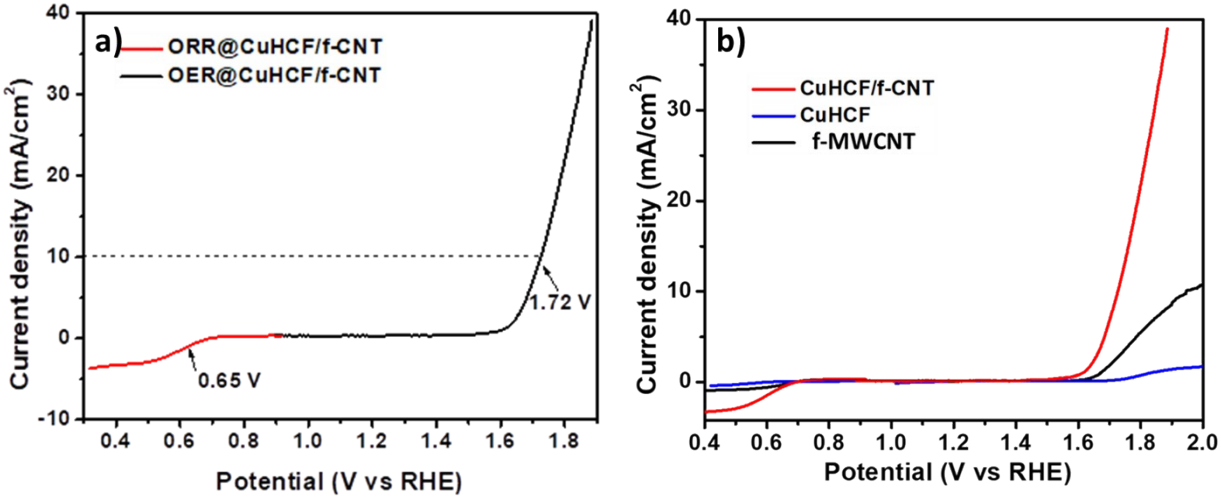

Fig. S10: **a)** The plot of ORR ($E_{1/2}$) and OER (10 mA/cm^2), with ΔE = 1.07 V vs RHE, **b)** Comparison plot for bifunctional OER/ORR activity for CuHCF, CuHCF/f-CNT and f-MWCNTs.

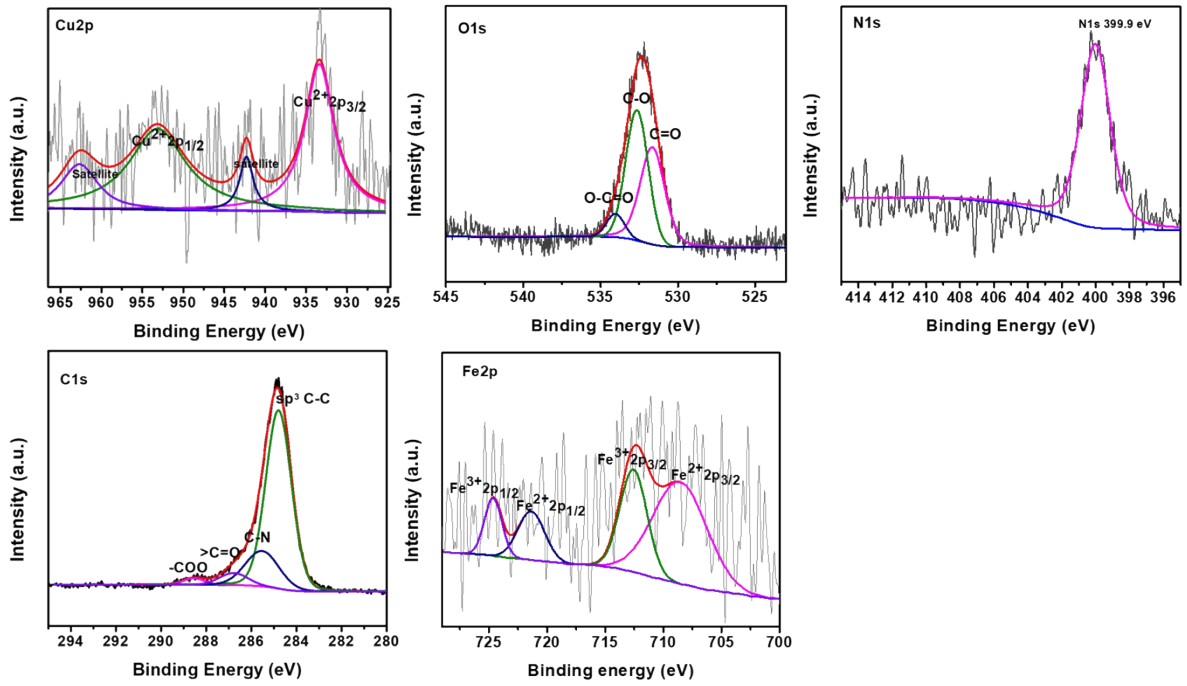

Fig. S11: XPS analysis of CuHCF/*f*-CNT after ORR analysis.

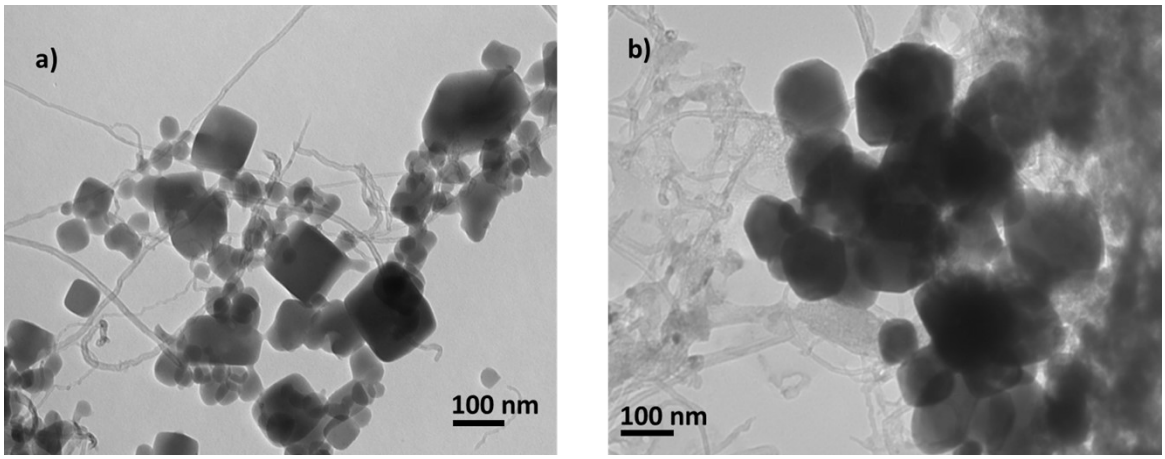

Fig. S12: TEM images of CuHCF/*f*-CNT before analysis (a) and after analysis (b)

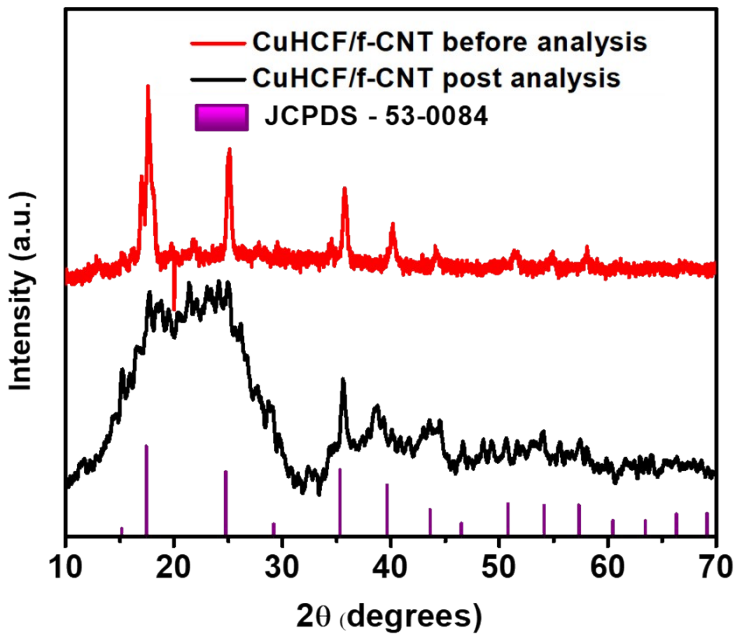

Fig. S13: XRD pattern before and after ORR analysis of CuHCF/*f*-CNT

Synthesis of Copper Hydroxide loaded MWCNTs:

For a comparison, the $Cu(OH)_2$/CNT composite was prepared using a simple reported co-precipitation strategy. In a typical procedure, 10 mg of f-MWCNTs were dissolved in 30 mL distilled water and was dispered using ultrasonicator. To the dispersion, 40 mM of $Cu(NO_3)_2.3H_2O$ was added followed by 15 mL of 0.3 M ammonia solution under constant magnetic stirring. A blue precipitate was produced by adding dropwise 50 mL, 1 M NaOH solution. The resulting precipitate was filtered and washed with distilled water and dried at room temprerature overnight.[8]

While following the same procedure used for the synthesis of CuHCF/f-CNT, but without the addition of iron presursor, i.e., $K_3[Fe(CN)_6]$, that resulted into CuO/f-CNT was also synthesized for comparison. In detailed procedure, 10 mg of f-MWCNT was dispersed in 30 mL distilled water follwed by addition of $Cu(NO_3)_2$ (40 mM) and then treated hydrothermally at 120 ^oC for 10 hours to obtain the precipitate. The resulted product was washed and dried before using it for electrochemical measurements.

XRD Analysis: The PXRD diffraction peaks of as synthesized $Cu(OH)_2$/CNT is shown in Fig. S17 (a). From the PXRD pattern it can be observed that the peaks matches with the standard XRD pattern of orthorhombic $Cu(OH)_2$ (PDF – 35-0505) showing sharp, high crystalline peaks without any impurity peaks. The main peaks at 2θ, 16.7°, 23.8°, 34.1°, 35.9°, 39.7°, 53.3°, and

63.0°, corresponds to the orthorhombic planes as assigned in the Fig. S17 (a).[8] In the PXRD pattern of as prepared CuO/f-CNT (Fig. S17 c), the XRD pattern matches with the standard CuO (PDF -892531).

FTIR Analysis: The FTIR spectrum of Cu $(OH)_2$/CNT is shown in Fig. S17b), the peak at 3313 and 3568 cm^{-1} is assigned to the OH- ions, the broad band at 3426 cm^{-1} and a peak at 1640 cm^{-1} is attributed to the OH stretching and bending modes in H_2O, respectively. The C-H vibration in evident from the peak at 1383 cm^{-1}. The absorption peak at 689.5 cm^{-1} is for Cu-O vibrations.[9]

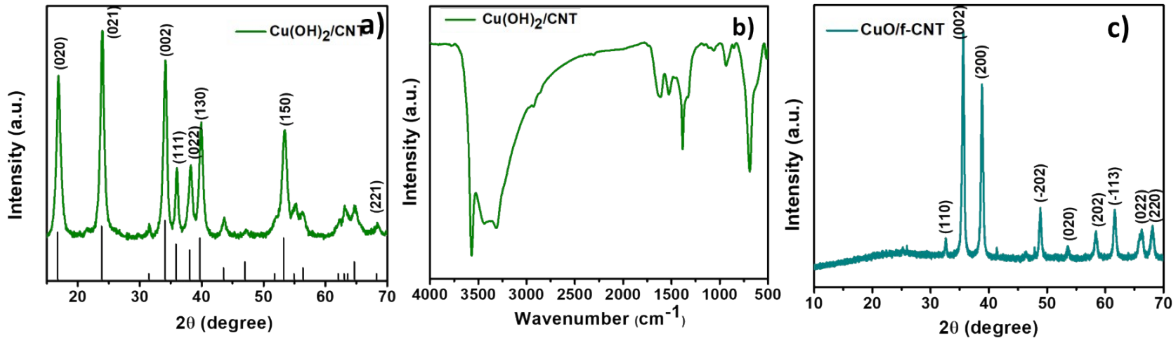

Fig. S14: a) PXRD pattern of $Cu(OH)_2$/CNT and standard XRD pattern of $Cu(OH)_2$ (PDF – 35-0505) b) FTIR spectra for as synthesized $Cu(OH)_2$/CNT, c) PXRD pattern of CuO/f-CNT.

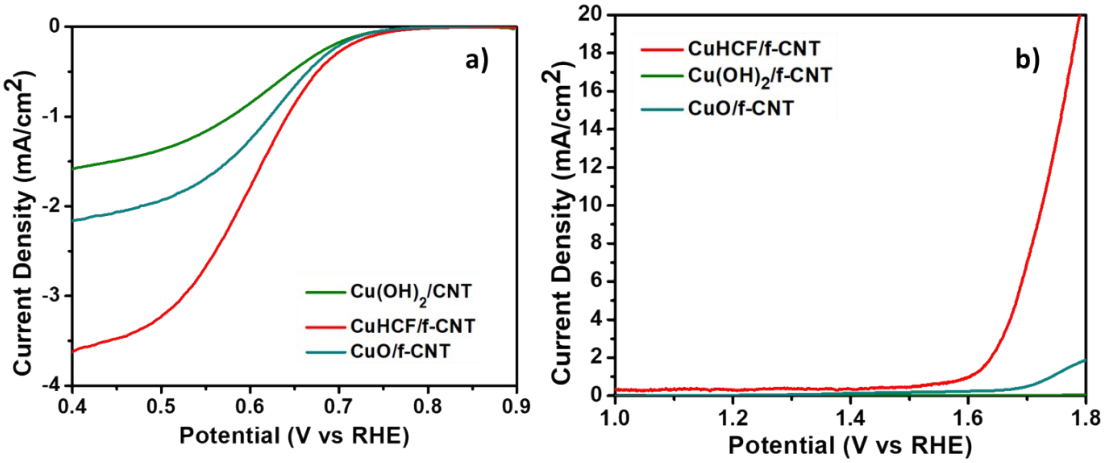

Fig. S15: The comparison of LSV polarisation curves for the a) ORR activity and b) OER activity of CuHCF/*f*-CNT and $Cu(OH)_2$/CNT.

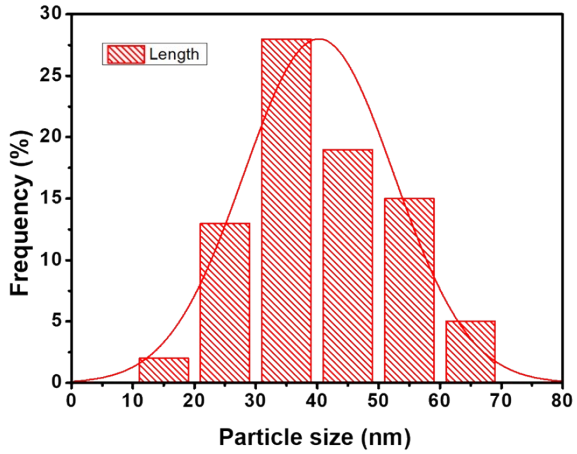

Fig. S16: Particle size distribution corresponding to TEM image in **Fig 3** for CuHCF/f-CNT.

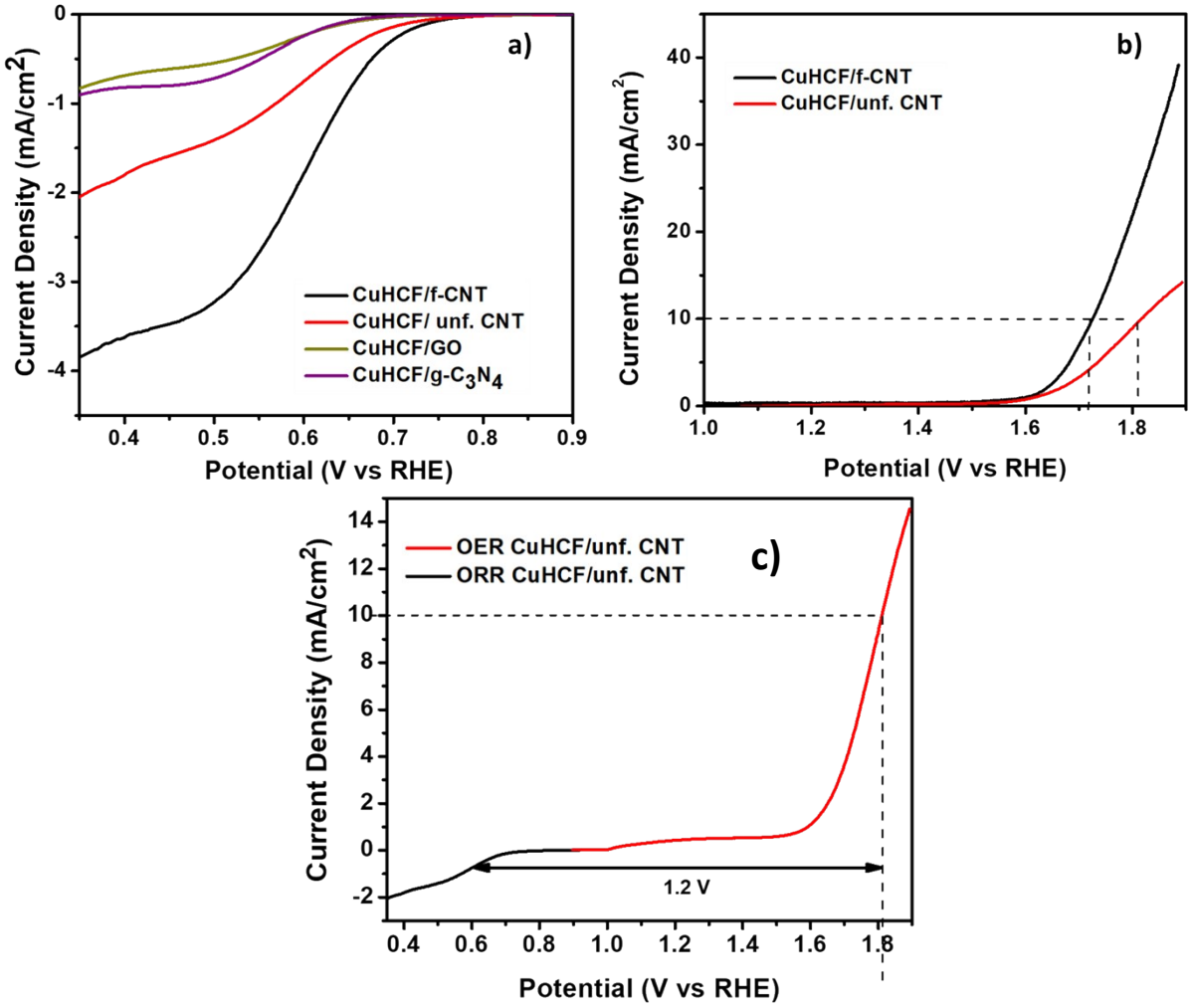

Fig. S17: The comparison plots for CuHCF/f-CNT and

CuHCF/unf. CNT. a) LSV ploarisation curve in O_2 saturated 0.1 M KOH for ORR activity, b) LSV curve comparison in 0.1 M KOH for OER activity, c) Bifunctional activity of CuHCF/unf. CNT in terms of ΔE.

References

1 T. Najam, M. Wang, M. S. Javed, S. Ibraheem, Z. Song, M. M. Ahmed, A. ur Rehman, X. Cai and S. S. A. Shah, *J. Colloid Interface Sci.*, 2020, **578**, 89–95.

2 H. T. Bui, N. K. Shrestha, K. Cho, C. Bathula, H. Opoku, Y. Y. Noh and S. H. Han, *J. Electroanal. Chem.*, 2018, **828**, 80–85.

3 J. Sanetuntikul and S. Shanmugam, *Electrochim. Acta*, 2014, **119**, 92–98.

4 H. Wang, L. Wei, B. Duan, J. Liu and J. Shen, *J. Electroanal. Chem.*, 2020, **877**, 114556.

5 L. Xu, G. Zhang, J. Chen, Y. Zhou, G. Yuan and F. Yang, *J. Power Sources*, 2013, **240**, 101–108.

6 N. K. Shrestha, H. T. Bui, S. J. Yoon, S. A. Patil, C. Bathula, K. Lee, Y. Y. Noh and S. H. Han, *J. Electroanal. Chem.*, 2019, **847**, 113179.

7 B. Zakrzewska, B. Dembinska, S. Zoladek, I. A. Rutkowska, J. Żak, L. Stobinski, A. Małolepszy, E. Negro, V. Di Noto, P. J. Kulesza and K. Miecznikowski, *J. Electroanal. Chem.*, , DOI:10.1016/j.jelechem.2020.114347.

8 S. Cui, X. Liu, Z. Sun and P. Du, *ACS Sustain. Chem. Eng.*, 2016, **4**, 2593–2600.

9 S. H. Park and H. J. Kim, *J. Am. Chem. Soc.*, 2004, **126**, 14368–14369.